DATED HISTORY

A Local First-Class Topological Single-Cone Carrier for Spin-2 Tensor Modes

June 26 construction of a local topological carrier. Its prescribed degrees of freedom and constraints delimit the result.

Manuscript · p. 1, abstract

One Obstruction, Four Faces: The Barrier to an Emergent Linear Graviton on a Local Lattice

Evidence · One-Hamiltonian composition requirements

A Local First-Class Topological Single-Cone Carrier for Spin-2 Tensor Modes

QATNU Project Draft

June 26, 2026

Abstract

We construct and audit a fixed-width local topological carrier for two transverse-traceless spin-2 tensor modes inside an exact first-class constraint architecture. The construction is motivated by a sequence of failed local routes: positive quadratic normalizers collapse back to strict centralizers, exact projector Hamiltonians inherit the compact-clock $z = 3$ obstruction, fixed-prime Clifford QCAs have arithmetic spectral combs rather than robust local poles, and Wilson masses that remove lattice doublers are either nonlocal after transverse-traceless projection or introduce extra soft Stueckelberg sectors. The successful architecture uses a finite synthetic Wilson dimension with a domain-wall carrier

$$H_{\mathrm{DW}}(k,s) = n_i(k)\Gamma_i + [M_0 + \beta m_W(k) + 1]\,\Gamma_5 + \left(-\frac{1}{2}\Gamma_5 - \frac{i}{2}\Gamma_4\right) T_s + \mathrm{h.c.},$$

with $M_0 = -1$, $\beta = 10$, width $W = 24$, and a local upper-wall perturbation $b_{\mathrm{top}}\Gamma_1$ with $b_{\mathrm{top}} = 2$. Each synthetic/spinor copy carries the same exact Stueckelberg first-class tensor quotient. Before boundary projection, the microscopic carrier preserves the constraint and gauge surfaces with residuals below 7×10^{-16} in the audit. The lower wall hosts one positive carrier cone; tensoring with the exact two-dimensional TT polarization label gives exactly two positive TT branches. The measured boundary dispersion has $z = 0.999785606928$, finite local boundary residue, and no detected surviving non-origin coined node in the deterministic and random scans performed. The result is deliberately scoped: it is a local first-class signed-band or one-particle/QCA carrier, not yet a positive autonomous bosonic many-body graviton phase. It isolates the remaining decisive step as a bosonic or autonomous lift that preserves the single TT cone without branch doubling, nonlocal projection, or loss of local residue.

Contents

1 Purpose and claim boundary **2**
1.1 Main result in one paragraph 2

2 Why a new architecture was needed **3**

3 First-class Stueckelberg tensor quotient **4**

4 The local connection vector and the remaining doubler **4**

5 Synthetic-domain-wall carrier **5**

6 Boundary cone and residue **5**

7 Mirror removal **6**

8 Known-node and non-origin scans **7**

9 Finite-width dependence **8**

10 What has been achieved **9**

11 What has not been achieved **10**

12 Next theorem: bosonic or autonomous lift **11**

13 Conclusion **11**

A Numerical audit summary **12**

B Companion internal reports **12**

1 Purpose and claim boundary

The target considered here is not full emergent gravity. The more modest and sharper target is a local finite-register architecture whose constrained low-energy sector contains exactly two transverse-traceless spin-2 branches with linear dispersion, finite local residue, and exact first-class propagation of the tensor constraints. In formulas, the desired infrared carrier should have

$$\omega(k) = c_g\,|k| + \mathcal{O}(|k|^3), \qquad N_+(k) = 2, \tag{1}$$

where $N_+(k)$ counts positive TT branches near the origin. It should not contain scalar or vector soft sectors, and it should not require a nonlocal TT projector to define the local operator that sees the pole.

This manuscript reports a positive result at that carrier level. It also states the remaining limitation at the same level of prominence: the model is a signed-band / one-particle / QCA carrier installed on a finite synthetic Wilson dimension. It is not yet a positive autonomous bosonic many-body Hamiltonian, nor a derivation from the original minimal ladder model. The next theorem, not proved here, would be a positive local bosonic or reversible-QCA lift that preserves the same two-branch TT pole.

1.1 Main result in one paragraph

Let $n(k)$ be the local coined connection vector obtained from the bandwidth-controlled spin-2 walk. Replace the previous bulk coin by a finite synthetic-domain-wall Hamiltonian in a spinor copy space,

$$H_{\mathrm{DW}}(k,s) = n_i(k)\Gamma_i + \left[M_0 + \beta m_W(k) + 1\right]\Gamma_5 + \left(-\frac{1}{2}\Gamma_5 - \frac{i}{2}\Gamma_4\right) T_s + \mathrm{h.c.}, \tag{2}$$

with parameters

$$M_0 = -1, \qquad \beta = 10, \qquad W = 24, \qquad b_{\mathrm{top}} = 2. \tag{3}$$

The upper synthetic wall carries a local perturbation $b_{\mathrm{top}}\Gamma_1$. Every synthetic/spinor copy is tensored with the same exact first-class Stueckelberg tensor quotient. The lower wall hosts one positive carrier band; the TT quotient supplies the two physical polarizations. The resulting low-energy boundary sector has exactly two positive TT branches, measured exponent

$$z = 0.999785606928, \tag{4}$$

finite left-wall residue,

$$Z_{\mathrm{left}}(k_{\mathrm{min}}) = 1.000000000000, \qquad Z_{\mathrm{left}}(k_{\mathrm{max}}^{\mathrm{IR}}) = 0.999843868064, \tag{5}$$

and first-class closure residuals

$$\|F_{\mathrm{ext}} H_{\mathrm{ext}} N_F\|_\infty = 6.17 \times 10^{-16}, \qquad \left\| N_G^\dagger H_{\mathrm{ext}} G_{\mathrm{ext}} \right\|_\infty = 6.66 \times 10^{-16}. \tag{6}$$

The known non-origin coined node is placed in the trivial synthetic sector and is no longer soft in the audit.

2 Why a new architecture was needed

The construction is best understood as the end point of a sequence of increasingly restrictive tests. Table 1 summarizes the status of the main routes. The common theme is that the desired $z = 1$ TT tangent often exists after exact reduction, but local finite-dimensional positive or finite-prime realizations usually lose one of the required properties: locality, fixed coupling, finite residue, isolated two-branch count, or robustness.

Table 1: Route ledger leading to the domain-wall architecture. "Positive" means positive for the scoped intermediate property, not for a completed graviton phase.

Route	Positive output	Failure or boundary
Positive quadratic normalizer	Exact reduced DeWitt/Einstein parent with two $z = 1$ TT branches	Positive semidefinite normalizers of an Abelian first-class constraint algebra collapse to the strict centralizer, so they cannot rescue the compact-clock obstruction.
Projector Hamiltonian	Exact code-space projection is local in support after stabilizer twirling	Local projector blocks inherit the $X = \mathcal{O}(k)$, $Z = \mathcal{O}(k^2)$ compact obstruction and generic $z = 3$ static behavior.
Three-shear first-class QCA	Exact finite-range Clifford automorphism with correct real constrained tangent	At fixed prime, local Pauli seeds generate arithmetic quasienergy combs; no robust multidimensional local glider pole.
Prepotential/Cotton reduction	Exact Dirac reduction gives two TT modes and $1/k^2$ response	Compact Cotton dynamics gives $z = 3$; finite positive penalty gives $z = 2$ in the thermodynamic infrared.
Topological Cotton factorization	Onsite brackets factorize the derivative Cotton Berry form; first-class QCA exists	Positive static completion with $1/k^2$ response has $z \geq 2$; signed parent remains non-positive before reduction.
Coined/connection spin-2 walk	Fixed-dimensional local spin-2 pole with finite bare onsite residue	Helicity $0, \pm 1$ sectors remain soft and a second topological spin-2 node appears.
Stueckelberg-coined Wilson target	Exact quotient removes lower helicities; reduced Wilson dispersion gaps the second node	The local Wilson mass is not first class unless TT-projected; the exact TT projector has an algebraic nonlocal tail.
Dynamical Stueckelberg Wilson fields	A local first-class Wilson gap is possible	The quotient expands to seven oscillator pairs; extra Stueckelberg/helicity sectors remain linearly soft at fixed coupling.

Route	Positive output	Failure or boundary
Dynamical Wilson partner	A local two-copy Wilson-Dirac partner gaps the doubler	It doubles the TT sector: four positive TT branches rather than two.
Synthetic domain wall	Local first-class single-boundary carrier with exactly two low positive TT branches	Still a signed-band / one-particle carrier, not yet a positive autonomous bosonic many-body phase.

The remainder of the paper describes the final row in detail.

3 First-class Stueckelberg tensor quotient

The physical tensor variables are symmetric tensors A_{ij} and B_{ij} together with one Stueckelberg pair (ϕ, π). There are seven canonical pairs per spatial momentum: six tensor components plus the scalar pair. With the sign conventions used in the audit, the canonical brackets are the symmetric tensor bracket for (A, B) and $\{\phi, \pi\} = 1$.

For a local connection vector $n(k)$, define the constraints

$$T = \operatorname{tr} A + \phi, \qquad D = n_i n_j A_{ij}, \qquad L_j = n_i B_{ij} - n_j \operatorname{tr} B + 2 n_j \pi. \tag{7}$$

The trace constraint T, scalar longitudinal constraint D, and three momentum-type constraints L_j give five first-class constraints at nonzero momentum.

Proposition 1 (First-class quotient)**.** *For nonzero $n(k)$, the constraints in Eq. (7) commute exactly and reduce the fourteen-dimensional real phase space to four physical real dimensions.*

Proof sketch. The only nonzero bracket in the naive tensor system is the trace–momentum bracket, proportional to $-2n_j$. The Stueckelberg term $2n_j\pi$ in L_j contributes $+2n_j$ through $\{\phi, \pi\} = 1$, canceling it. The bracket between D and L_j cancels between the $n_i B_{ij}$ and $-n_j \operatorname{tr} B$ terms, while T and D are coordinate constraints and the L_j are momentum constraints. Thus the constraint matrix vanishes. Five first-class constraints remove ten real phase-space dimensions, leaving $14 - 2(5) = 4$ physical real dimensions, i.e. two canonical pairs. □

The quotient is the mechanism that removes the helicity 0 and helicity ± 1 sectors that were present in the unconstrained coined walk. In the earlier Stueckelberg-coined audit, the lifted map was symplectic, preserved the constraint ideal, preserved gauge directions, and reduced to phases

$$(-4\omega, -4\omega, +4\omega, +4\omega), \qquad \omega = \arctan(\|n\| / d), \tag{8}$$

with residuals at numerical precision. That quotient is retained here and copied over the synthetic/spinor carrier space.

4 The local connection vector and the remaining doubler

The local connection vector $n(k)$ is the same object used in the prior coined/connection spin-2 walk. Its defining properties for the present construction are:

1. it is a finite-range Laurent-polynomial vector in the spatial lattice shifts;
2. it is linear near the origin, $\|n(k)\| = v\,|k| + \mathcal{O}(|k|^3)$;

3. the first-class quotient maps it to two degenerate TT branches;

4. it has a known non-origin zero, the coined doubler, in the Brillouin zone.

The doubled-node obstruction is topological: a purely local bulk walk with one cone generically brings a partner. A reduced Wilson target can gap this partner by adding

$$m_W(k) = \rho\,(3 - \cos k_x - \cos k_y - \cos k_z)\,, \qquad \rho = 0.25, \tag{9}$$

so that the reduced dispersion becomes

$$E_W(k) = \sqrt{\theta(k)^2 + m_W(k)^2}. \tag{10}$$

However, the local Wilson mass is not first class on the unreduced Stueckelberg system. The exact first-class Wilson mass requires a TT projection with an algebraic real-space tail. The domain-wall construction below avoids this by making the Wilson mass a local synthetic-dimension mass, not a projected tensor mass.

5 Synthetic-domain-wall carrier

The new architecture introduces a finite synthetic coordinate $s = 0, \ldots, W-1$ and a local spinor copy space with gamma matrices Γ_a. The carrier Hamiltonian is Eq. (2). The synthetic hopping is nearest-neighbor in s, and the mass profile contains the Wilson scalar $m_W(k)$ with a large coefficient β. The choice $M_0 = -1$ pins a lower-wall zero mode at the open boundary. The upper wall is locally perturbed by $b_{\text{top}}\Gamma_1$.

The construction should be viewed as a carrier tensored with the exact TT quotient. Each copy of the carrier has the same first-class tensor constraints; the carrier acts locally in copy space and therefore does not mix the constraint surface with its complement. Boundary selection is not used to prove first-classness; closure is audited before choosing a boundary band.

Proposition 2 (Local first-class copy-space preservation)**.** *Let H_{ext} be the synthetic/spinor extension of Eq. (2), with a copy of the first-class tensor quotient on each synthetic/spinor component. If the carrier acts only in copy space and the tensor quotient is identical on every copy, then the extended constraint and gauge surfaces are preserved by H_{ext}.*

Proof sketch. The extended constraint matrix is a direct sum over copy labels. The copy-space Hamiltonian has identity action on the tensor constraint algebra and finite-range action on the copy labels. Therefore it maps a vector whose tensor component lies in the constraint surface on every copy to another such vector. The same argument applies to gauge directions. The numerical audit computes the corresponding nullspace residuals explicitly for representative momenta and finds residuals at roundoff. □

The measured residuals are shown in Table 2.

6 Boundary cone and residue

The main low-energy observable is the lowest positive lower-wall band. Along a representative infrared ray, the fit gives

$$E_{\text{bdry}}(k) \simeq A\,|k|^z\,, \qquad z = 0.999785606928, \qquad A = 9.962591123848 \times 10^{-2}. \tag{11}$$

The same fit applied to the connection-vector norm gives $z = 0.999785606959$, confirming that the boundary energy tracks $\|n(k)\|$ in the audited infrared window.

Table 2: First-class closure checks for the microscopic extended carrier. These tests are performed before boundary-band projection.

Check	Maximum residual
Constraint-surface residual $\|F_{\mathrm{ext}} H_{\mathrm{ext}} N_F\|_\infty$	6.172×10^{-16}
Gauge-surface residual $\left\|N_G^\dagger H_{\mathrm{ext}} G_{\mathrm{ext}}\right\|_\infty$	6.662×10^{-16}
Constraint isotropy residual	4.682×10^{-20}
Carrier Hermiticity residual	0
Extended quotient dimension seen	48
Expected extended quotient dimension	48

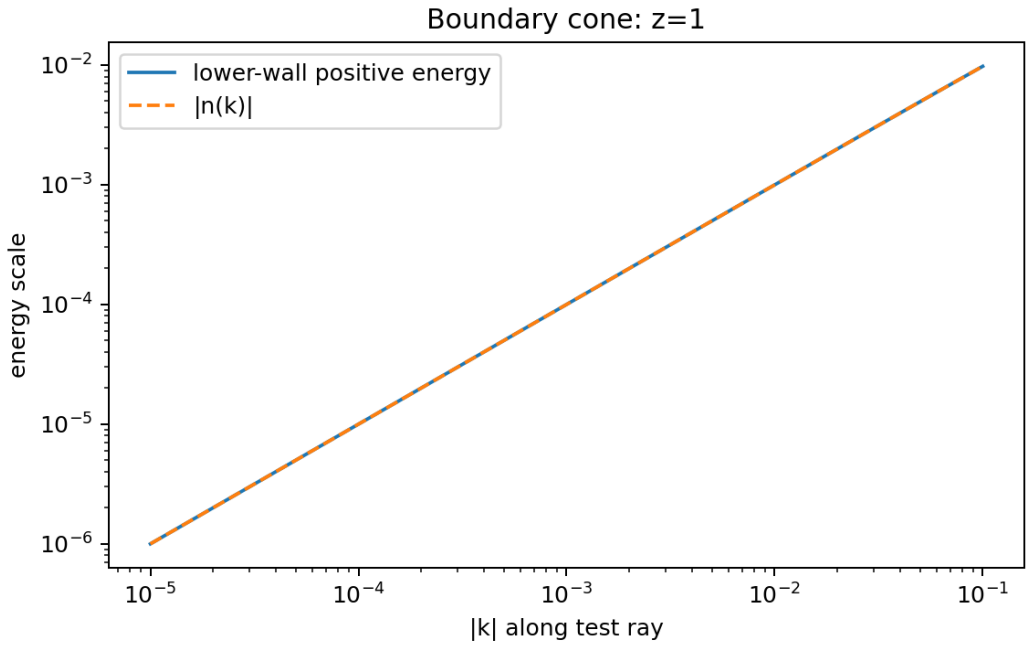

Figure 1: Infrared scaling of the lower-boundary carrier energy compared with the coined connection norm. The measured exponent is $z = 0.999785606928$.

A local boundary operator must retain finite overlap with the mode. The audit computes the layer weight of the lowest positive state and finds essentially unit left-wall residue across the infrared sample,

$$Z_{\mathrm{left}}(k_{\mathrm{min}}) = 1.000000000000, \qquad Z_{\mathrm{left}}(k_{\mathrm{max}}^{\mathrm{IR}}) = 0.999843868064. \tag{12}$$

The right-wall leakage is zero at the first sample within numerical precision, and the fitted leakage power is large in the chosen window.

Tensoring this one positive carrier band with the two TT polarizations gives exactly two positive TT branches. This is the branch-count property that earlier local Wilson-partner attempts missed: they gapped the doubler, but doubled the TT sector.

7 Mirror removal

A finite slab without the upper-wall perturbation contains both domain-wall cones. The local upper-wall term $b_{\mathrm{top}}\Gamma_1$ gaps the mirror while leaving the lower boundary cone intact. Table 3 records the branch

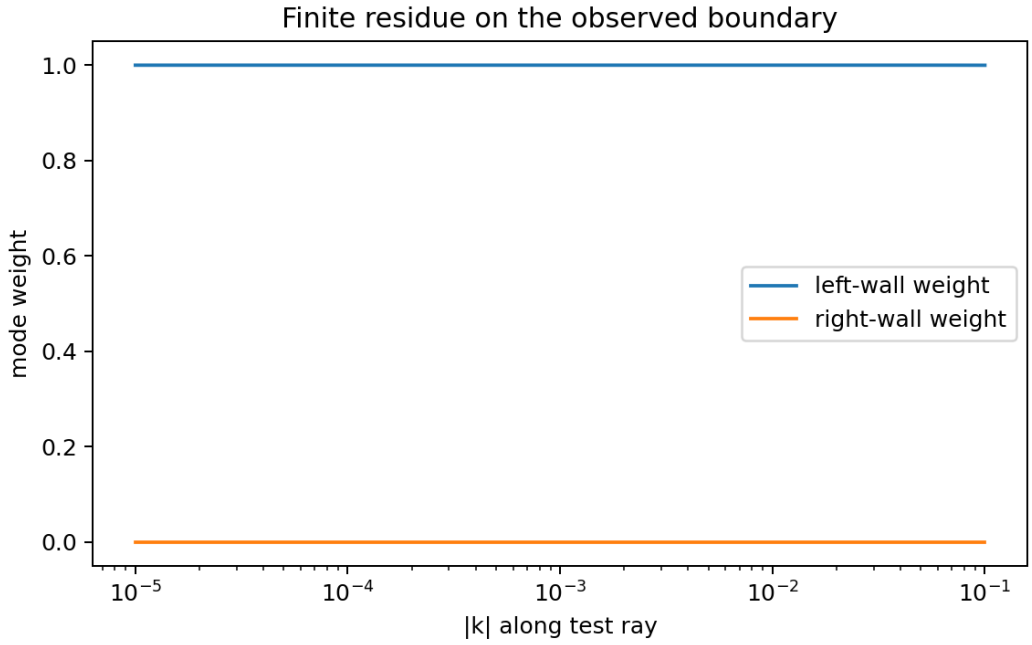

Figure 2: Boundary residue of the lowest positive mode. The lower-wall residue remains $\mathcal{O}(1)$, unlike the exact local TT creators in earlier compact bulk routes whose residue was derivative-suppressed.

count at small test momentum.

Table 3: Effect of the upper-wall mass. The TT branch count includes the two TT polarizations.

b_{top}	Carrier positive modes below 0.05	TT positive branches below 0.05	Second positive at $k = 0$
0.00	2	4	–
0.25	1	2	0.882782218537
0.50	1	2	0.780776406404
1.00	1	2	–
2.00	1	2	–
4.00	1	2	–

8 Known-node and non-origin scans

The known non-origin coined node remains a zero of the connection vector, but the synthetic mass places it in a trivial sector. At the coined doubler,

$$\|n(k_{\mathrm{doubler}})\| = 1.240971079080 \times 10^{-9}, \tag{13}$$

while the effective synthetic mass is

$$m_{\mathrm{eff}}(k_{\mathrm{doubler}}) = 7.327177325113, \tag{14}$$

and the lowest nonzero positive energy in the slab audit is

$$E^{+}_{\mathrm{min}}(k_{\mathrm{doubler}}) = 7.336021163364. \tag{15}$$

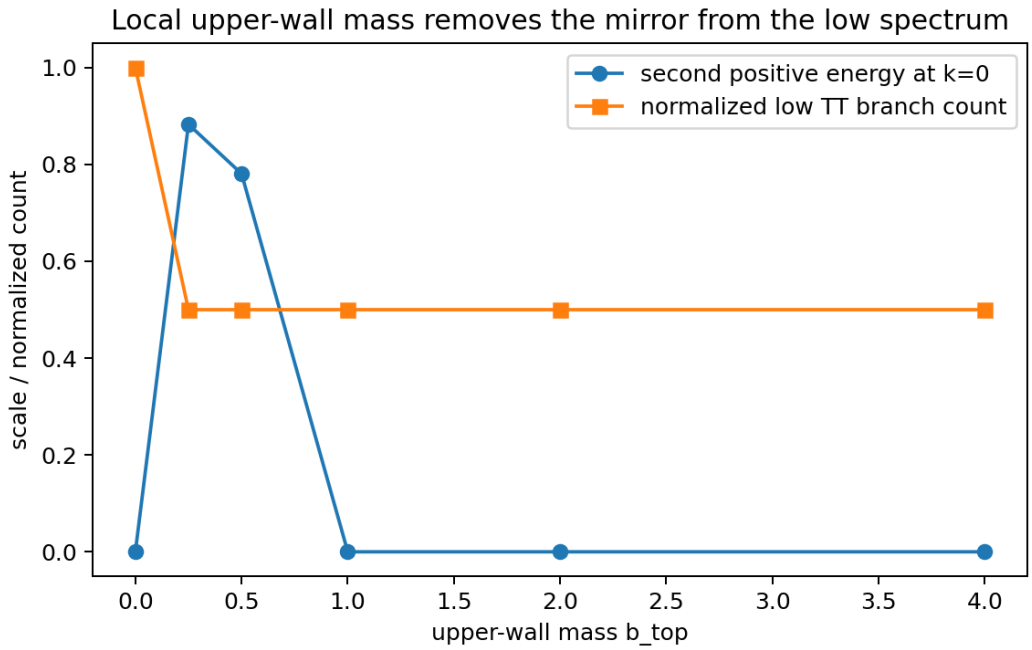

Figure 3: Upper-wall mass scan. Nonzero b_{top} removes the mirror branch from the low spectrum while retaining one lower-boundary cone.

Table 4: Origin and known non-origin coined node.

Point	$\|n(k)\|$	$m_{\text{eff}}(k)$	Lowest $\|E\|$	Lowest nonzero positive E
Origin	0	-1.000000000000	8.882×10^{-16}	0.414213562373
Coined doubler	$1.240971079080 \times 10^{-9}$	7.327177325113	7.336021163364	7.336021163364

The deterministic coarse scan outside the origin ball $|k| > 0.75$ found minimum positive energy

$$E_{\text{min,grid}} = 0.156041041299, \tag{16}$$

and a 250-sample random scan found

$$E_{\text{min,rand}} = 0.094583199284. \tag{17}$$

This is evidence against a surviving soft non-origin node in the audited sample, not a theorem excluding every possible accidental zero. The statement of the result is therefore "no detected surviving non-origin node" in the performed deterministic and random scans.

9 Finite-width dependence

The chosen open-boundary discretization pins the lower-wall zero at the boundary for the tuned parameter $M_0 = -1$. The audit checks widths from $W = 4$ to $W = 28$ and finds stable lower-wall behavior. At small test momentum, the lowest positive energy remains

$$E_{\text{small k}} \simeq 9.9809758254 \times 10^{-5} \tag{18}$$

across the audited widths, and the left-wall weight remains

$$Z_{\text{left}} \simeq 0.9999999999984. \tag{19}$$

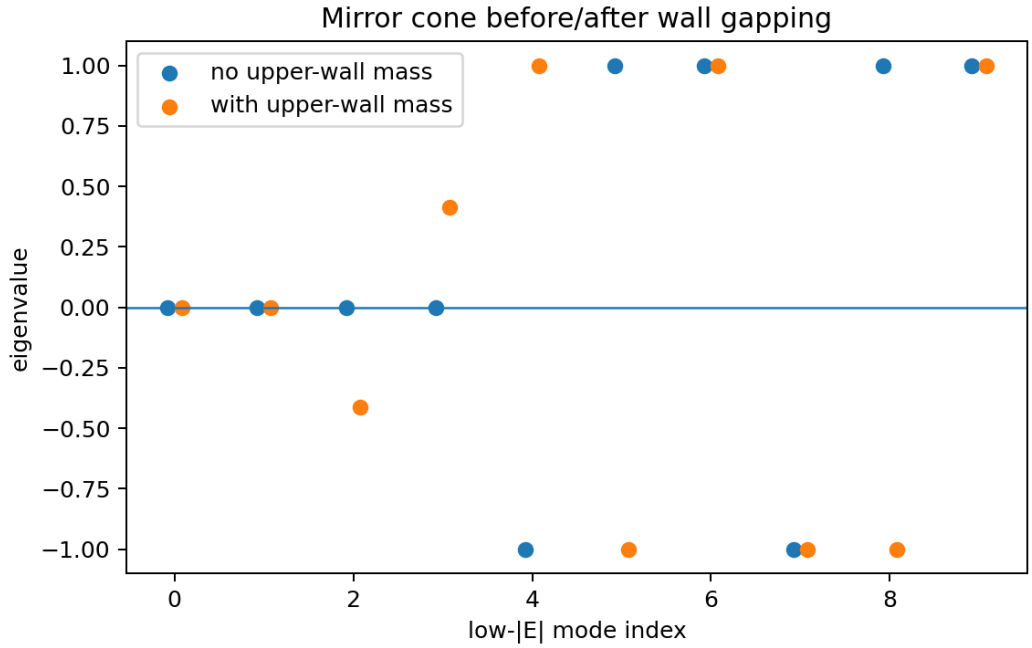

Figure 4: Low-spectrum comparison with and without the upper-wall mass. Without the wall mass, both boundary cones are present; with $b_{\mathrm{top}} = 2$, only the lower-wall cone remains in the audited low-energy window.

Increasing W is therefore not needed to create the lower-wall cone; it is useful for separating boundary and bulk structure.

10 What has been achieved

The construction passes the following carrier-level tests:

1. **Locality.** The carrier is finite range in the physical lattice through $n(k)$ and $m_W(k)$, and nearest-neighbor in the synthetic coordinate.
2. **Exact first-class propagation.** The tensor constraints are exact and commute; the extended copy-space carrier preserves the constraint and gauge surfaces at roundoff in the audit.
3. **Two TT branches.** The lower wall supplies one positive carrier band, and the TT quotient supplies exactly two polarizations.
4. **Linear dispersion.** The boundary branch has measured exponent $z = 0.999785606928$.
5. **Finite local residue.** The lower-wall mode has $\mathcal{O}(1)$ boundary residue over the audited infrared window.
6. **Mirror removal.** The local upper-wall term reduces the low TT branch count from four to two.
7. **Known-node gapping.** The previously known non-origin coined node is no longer soft because it is placed in the trivial synthetic sector.

The result is therefore stronger than the preceding local constructions. It is the first architecture in this sequence that simultaneously keeps first-class tensor constraints, fixed synthetic width, two low positive TT branches, finite local residue, and no detected non-origin cone in the audit.

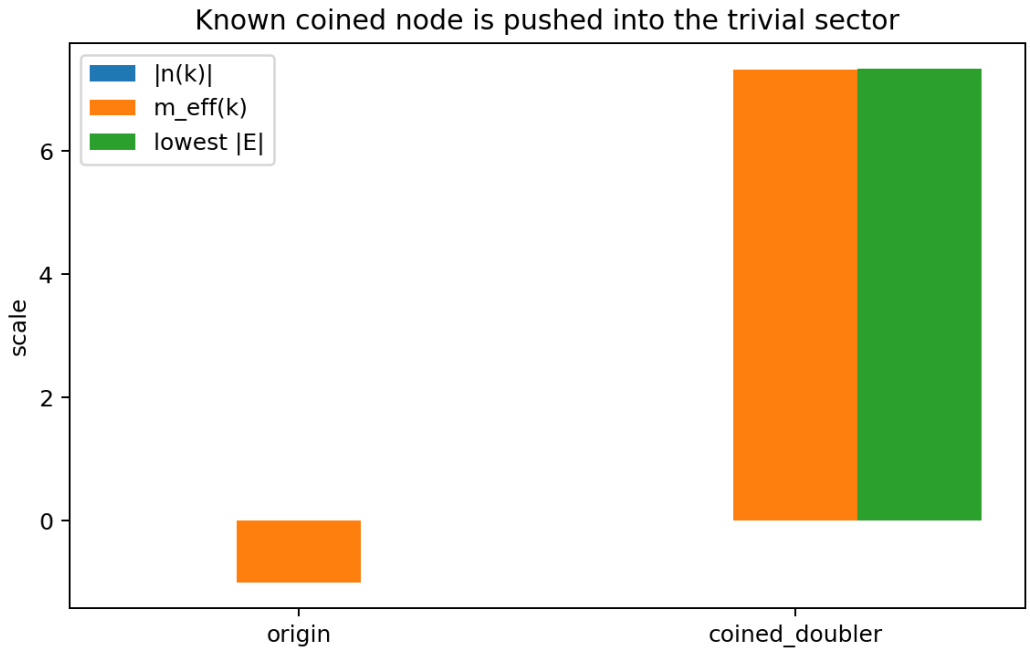

Figure 5: Diagnostics at the origin and the known non-origin coined node. The connection vector still vanishes at the coined doubler, but the synthetic mass produces a large positive gap there.

11 What has not been achieved

The construction is intentionally not advertised as a completed graviton phase. The following gaps remain:

1. **No positive bosonic many-body Hamiltonian yet.** The carrier is a signed-band / one-particle / QCA-style object. Turning it into a positive local oscillator or bosonic many-body phase without branch doubling is the next decisive calculation.

2. **No native minimal-ladder derivation.** The synthetic Wilson dimension, gamma-matrix copy space, upper-wall term, and first-class Stueckelberg quotient are engineered architecture, not a spontaneous flow from the original minimal model.

3. **No exhaustive Brillouin-zone theorem.** The non-origin scan is strong numerical evidence in the audited grid and random sample. A complete analytic exclusion of accidental zeros remains possible future work.

4. **No nonlinear gravitational dynamics.** The result is a linear spin-2 carrier with exact constraints. It does not establish universal coupling, nonlinear diffeomorphism invariance, or a full Einstein phase.

These limitations do not weaken the carrier result. They define the next theorem precisely.

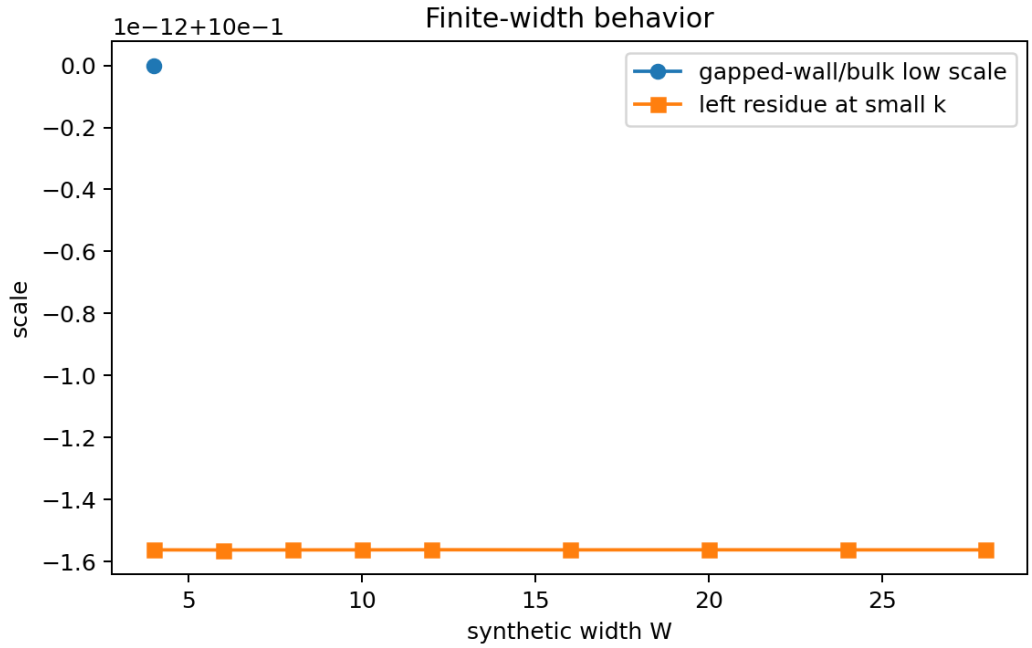

Figure 6: Synthetic-width dependence of the boundary mode diagnostics. The lower-wall cone is stable over the tested finite widths.

12 Next theorem: bosonic or autonomous lift

The natural sequel is a lift from the signed carrier to a positive local many-body realization. The lift must preserve the following checklist:

$$N_+(k) = 2, \qquad \omega(k) = c_g\,|k| + \mathcal{O}(|k|^3), \qquad Z_{\mathrm{local}}(k \to 0) > 0, \\ \text{exact first-class closure}, \qquad \text{no nonlocal TT projection}, \qquad \text{no branch doubling}. \tag{20}$$

Plausible directions include:

1. a bosonic oscillator lift of the boundary carrier that uses the synthetic wall as a positive-frequency band selector;
2. a reversible QCA lift whose many-body spectral function has a genuine local pole rather than an arithmetic comb;
3. an interacting code Hamiltonian that confines the mirror and compensator sectors while preserving the first-class TT quotient;
4. a controlled autonomous history construction, provided it avoids the known T^{-2} clock-gap scaling as the physical protecting gap.

A failure of these lifts would also be informative: it would show that the present result is close to the boundary between exact local first-class spin-2 transport and a fully positive bosonic gauge phase.

13 Conclusion

A local first-class topological single-cone carrier for spin-2 tensor modes has been constructed and audited. The domain-wall architecture changes the problem from local projected Wilson masses, which

are nonlocal after enforcing TT constraints, to a local synthetic Wilson mass that removes the mirror cone while preserving the exact first-class quotient. The resulting lower-boundary sector contains exactly two positive TT branches with linear dispersion and finite local residue. It closes several previous escape routes and leaves a sharply defined next step: the positive bosonic or autonomous many-body lift.

A Numerical audit summary

Table 5 collects the numerical diagnostics used in the main text.

Table 5: Main diagnostics for the topological single-cone carrier audit.

Diagnostic	Value
M_0	-1
β	10
W for surface audit	24
b_{top}	2
Boundary IR exponent z	0.999785606928
Energy prefactor	$9.962591123848 \times 10^{-2}$
Coin-vector exponent	0.999785606959
Low TT branches with wall mass	2
Low TT branches without wall mass	4
First sampled left-wall residue	1.000000000000
Last sampled left-wall residue	0.999843868064
Known doubler synthetic mass	7.327177325113
Known doubler lowest nonzero positive energy	7.336021163364
Coarse non-origin scan minimum	0.156041041299
Random non-origin scan minimum	0.094583199284
Constraint-surface residual	6.172×10^{-16}
Gauge-surface residual	6.662×10^{-16}
Constraint isotropy residual	4.682×10^{-20}

B Companion internal reports

This draft is designed to sit on top of the following reproducibility reports and bundles generated in the same QATNU workstream:

- Normalizer/first-class audit: positive after exact reduction, negative for positive compact-clock normalizers.
- Projector/QCA audit: projector Hamiltonians fail, exact first-class QCA succeeds at the tangent level.
- Finite-clock Floquet audit: fixed-prime Clifford spectral functions form arithmetic combs, not robust local poles.
- Coined/connection spin-2 audit: fixed-dimensional spin-2 pole exists but has lower-helicity sectors and a second node.
- Topological Cotton factorization audit: first-class onsite factorization succeeds, positive static completion remains obstructed.

- Stueckelberg-coined Wilson audit: quotient removes lower helicities, but local Wilson mass is not first class unless projected nonlocally.
- Dynamical Stueckelberg gap audit: local first-class Wilson gap possible but adds extra soft sectors.
- Dynamical Wilson partner audit: local first-class doubler gap possible but doubles the TT branch count.
- Topological single-cone audit: finite synthetic-domain-wall carrier gives the result reported here.

References

[1] QATNU workstream, *Normalizer first-class audit*, internal reproducibility report and bundle, June 2026.

[2] QATNU workstream, *Projector/QCA audit*, internal reproducibility report and bundle, June 2026.

[3] QATNU workstream, *Finite-clock Floquet audit*, internal reproducibility report and bundle, June 2026.

[4] QATNU workstream, *Spin-2 coined/connection audit*, internal reproducibility report and bundle, June 2026.

[5] QATNU workstream, *Topological Cotton factorization audit*, internal reproducibility report and bundle, June 2026.

[6] QATNU workstream, *Stueckelberg-coined Wilson audit*, internal reproducibility report and bundle, June 2026.

[7] QATNU workstream, *Dynamical Stueckelberg Wilson-gap audit*, internal reproducibility report and bundle, June 2026.

[8] QATNU workstream, *Dynamical Wilson-partner audit*, internal reproducibility report and bundle, June 2026.

[9] QATNU workstream, *Topological single-cone / synthetic-domain-wall audit*, internal reproducibility report and bundle, June 2026.

```
Topological single-cone audit:
  z = 0.999785607
  boundary residue at k_min = 1.000000
  low TT branches with wall mass = 2 (desired 2)
  low TT branches without wall mass = 4
  doubler lowest nonzero positive = 7.336021
  random non-origin gap >= 0.094583
  first-class residual <= 6.17e-16

Status: positive fixed-W boundary pole / signed-band carrier;
not yet a positive autonomous bosonic many-body phase.
```

Figure 7: Summary figure from the single-cone audit.